CHAPTER 3

RESULTS

3.1) Cloning of the lipase gene

3.1.1) Determination of the nucleotide sequence of the lipase P1

The lipase gene from *B. stearothermophilus* P1 had been cloned on 2.2 kb on *Sau* 3AI fragment into plasmid pUC-19 on *Bam* HI and transformed into *E. coli* DH5α. The nucleotide sequence of the gene was submitted to GenBank under accession number AF237623 and revealed an open reading frame of 1,254 bp encoding a 417 amino acid polypeptide (Fig. 3.1). It consisted of a 29 amino acid signal sequence and a mature lipase of 388 amino acid residues with a cleavage site between the two alanine residues at positions 29 and 30. This was confirmed by NH_2-terminal amino acid sequence analysis of the purified lipase showing that the first 15 amino acid residues had the sequence A-S-L-R-A-N-D-A-P-I-V-L-L-H-G.

3.1.2) Digestion with restriction enzymes

The plasmid DNA of the lipase gene was extracted and amplified with the primers lipase-F and lipase-R by using PCR. The obtained PCR product and pQE-60 as the expression vector were cleaned up with PCR clean up and partial digested with *Nco* I and *Hind* III as the restriction enzymes. The cutting plasmid DNA and pQE-60 were cleaned up with PCR clean up and then run on agarose gel electrophoresis. The result of DNA digestion was shown in Fig. 3.2. The cutting plasmid DNA of lipase

gene showed the nucleotide approximately 1.2 kb and the cutting pQE-60 showed the nucleotide approximately 3.4 kb.

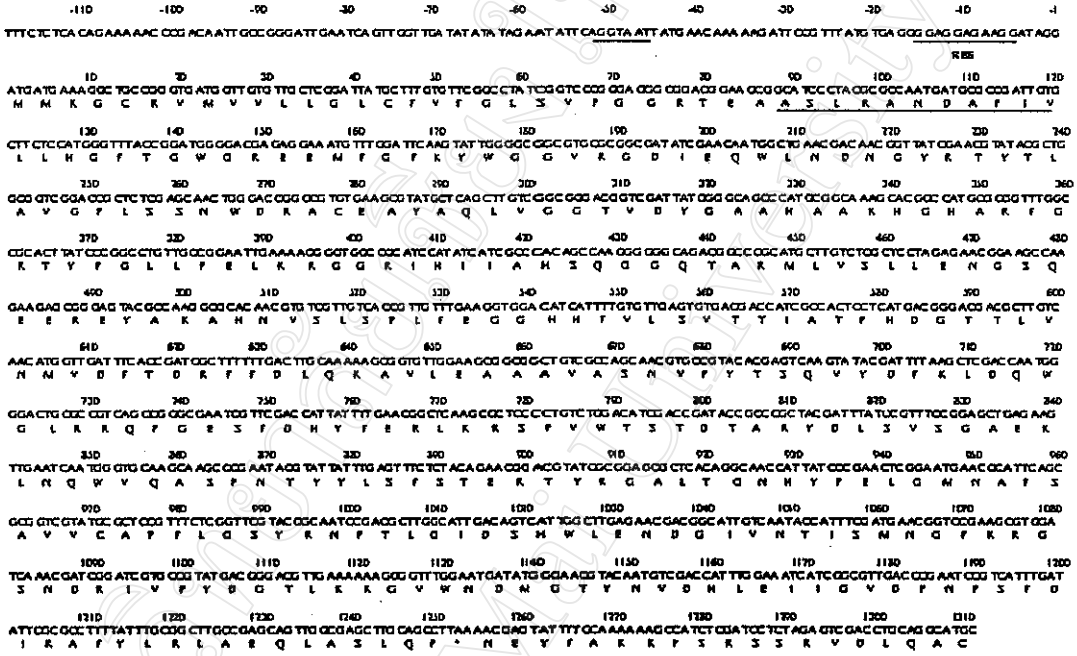

Fig. 3.1. Nucleotide sequence of the lipase gene from *B. stearothermophilus* P1 cloned in *E. coli* DH5α using pUC-P1 vector and its deduced amino acid sequence. The numbering of nucleotides starts at the 5′ end of the lipase gene and that of amino acids at the NH_2-terminus of the mature lipase. The putative –35, -10, and ribosomal binding sites (RBS), and stop codon (*) are shown. The NH_2-terminal amino acid sequence determined for the purified lipase P1 is underlined.

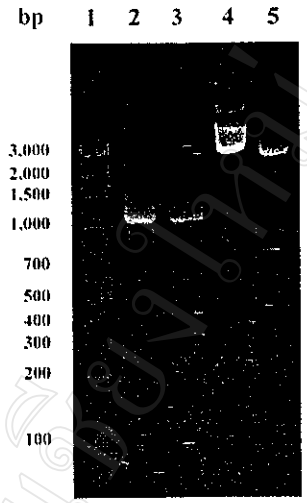

Fig. 3.2. Agarose gel electrophoresis shows the digestion of the lipase gene with restriction enzymes. Label: lane 1, DNA marker; lane 2, pUC-P1; lane 3, pUC-P1 cut with *Nco* I and *Hind* III; lane 4, pQE-60 (vector) and lane 5, pQE-60 cut with *Nco* I and *Hind* III.

3.1.3) Ligation, transformation and screening of recombinant lipase

After the lipase gene and pQE-60 were cut at the same restriction sites (*Nco* I and *Hind* III), they were ligated and transformed into the competent cell of *E. coli* M15[pREP4] and JM109. *E. coli* M15[pREP4] transformed with the vector containing the *B. stearothermophilus* P1 lipase coding sequence were selected by plating on LB agar containing 100 μg/ml of ampicillin, 25 μg/ml of kanamycin, and 1% (w/v) tricaprylin; colonies surrounded by a clear zone were selected and grown in the LB medium containing 100 μg/ml of ampicillin, 25 μg/ml of kanamycin. The recombinant DNA was isolated and amplified with the primers pQE-F and pQE-R and shown a 1.2 kb insert on agarose gel electrophoresis (Fig. 3.3). Otherwise, the inserted

DNA of the lipase gene was also confirmed by amplifying with the primers lipase-F and lipase-R and/or P1 and P2 and showed the same size of DNA on agarose gel electrophoresis. The recombinant lipase in *E. coli* JM109 was checked for the inserted DNA the same way as for the recombinant lipase in *E. coli* M15[pREP4] and also showed the same size of DNA on agarose gel electrophoresis. This plasmid designating as pQE-P1 was sequenced and shown to contain a 1.2 kb sequence coding for lipase. Its physical map was shown in Fig. 3.4.

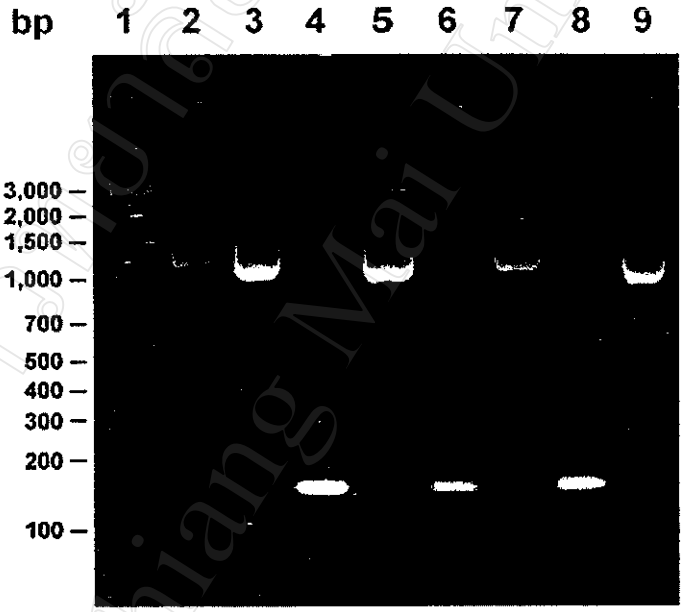

Fig. 3.3. Screening of recombinant lipase cloned in *E. coli* M15[pREP4] using pQE-60 as an expression vector on agarose gel electrophoresis. (Label: lane 1, DNA marker; lane 2, PCR product, and lane 3-9, recombinant lipase amplifying with pQE-F and pQE-R.)

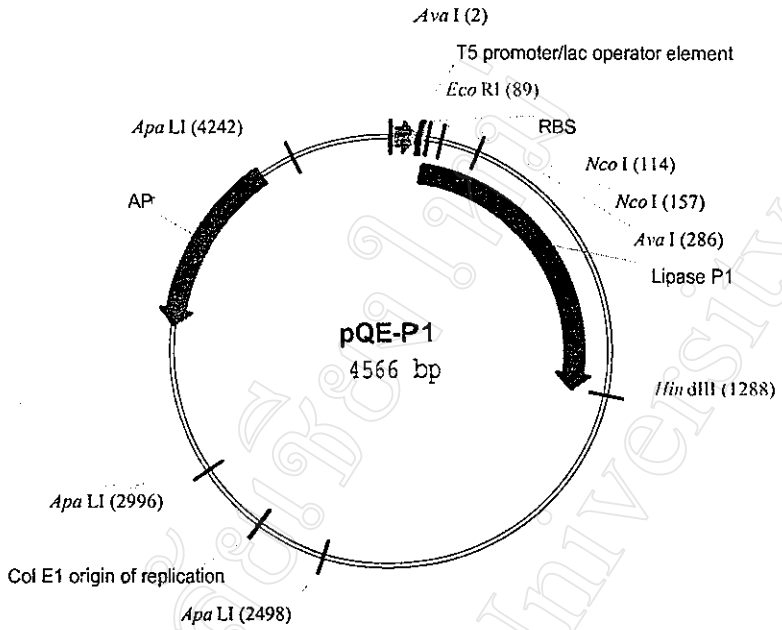

Fig. 3.4. Physical map of inserted lipase P1 after cloning of partial *Nco* I and *Hind* III fragments into pQE-60. The arrow indicates the region encoding the lipase gene and the direction of transcription.

3.1.4) Nucleotide sequence and NH_2-terminal amino acid sequence of the lipase gene cloned in *E. coli* M15[pREP4] using pQE-60 vector

The nucleotide sequence of the lipase gene from *B. stearothermophilus* P1 that was cloned on a 1.2 kb fragment into plasmid pQE-60 and host *E. coli* M15[pREP4] and JM109 revealed an open reading frame of 1,167 bp encoding a 388 amino acid polypeptide that had been submitted to GenBank under accession number AF237623 (Fig. 3.5). The NH_2-terminal amino acid sequence analysis of purified lipase showed that the first 15 amino acid residues had the sequence A-S-L-R-A-N-D-A-P-I-V-L-L-H-G. These results showed that the mature lipase lacked a signal peptide as a consequence of secretion across the outer membrane.

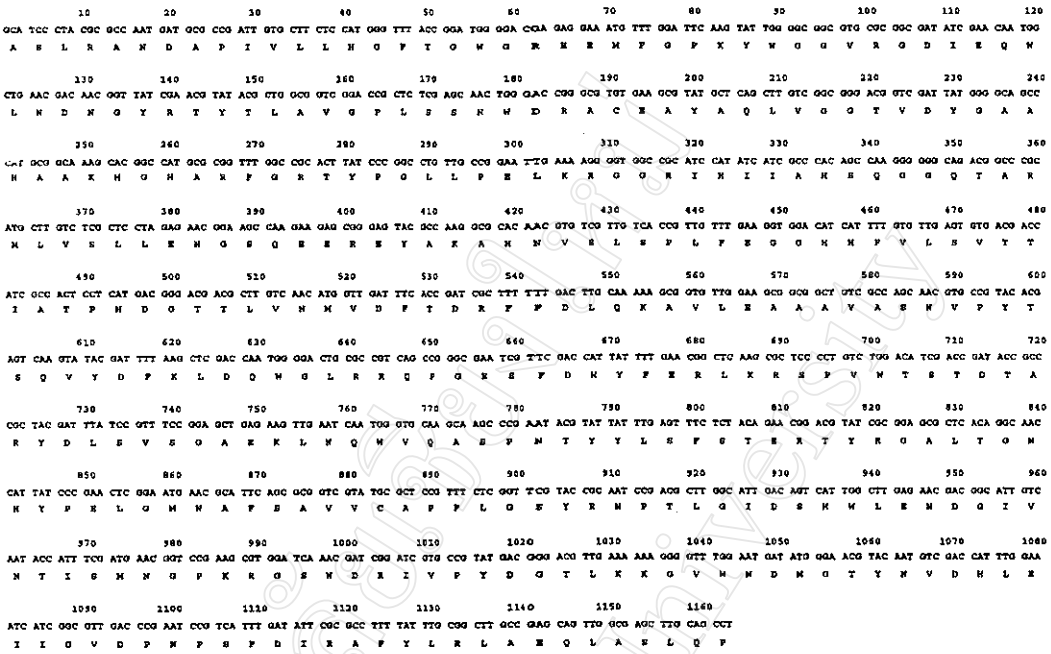

Fig. 3.5. Nucleotide sequence of the lipase gene from *B. stearothermophilus* P1 cloned into *E. coli* M15[pREP4] using pQE-60 as an expression vector. The numbering of nucleotides starts at the 5′ end of the lipase gene with the NH_2-terminus of the mature lipase at Ala.

3.2) Expression of the lipase gene in *E. coli*

When the lipase gene was optimized by cloning into *E. coli* M15[pREP4] and JM109, the expressions of the lipase between the native lipase P1 and the recombinant lipases were compared and shown in Table 3.1. All recombinant lipases in *E. coli* DH5α, M15[pREP4] and JM109 had the high lipase activity in the cell extract more than the supernatant. The lipase activities of the recombinant lipase in *E. coli* M15[pREP4] and JM109 were higher than the recombinant lipase in *E. coli* DH5α indicating that the changes of vector and host of the recombinant lipase could

optimize the lipase production. The expression of the recombinant lipase in *E. coli* M15[pREP4] in cell extract showed the highest lipase activity that higher than in *E. coli* DH5α and JM109. The overexpression of the cloned lipase P1 in *E. coli* M15[pREP4] resulted in a high expression of soluble lipase activity of 212×10^3 U/l compared with 8.1 U/l using the native lipase from *B. stearothermophilus* P1, i.e. a 26×10^3-fold increase.

Table 3.1. Comparison of the expressions of the native lipase P1 and the recombinant lipase P1 in the different vectors and hosts.

Enzymes	Activity ($\times10^3$ U/ml)	Total activity ($\times10^3$ U)	Total protein (mg)
Native P1 – extracellular	0.0081	0.81	0.01
Cloned pUC-P1 in DH5α – extracellular	0.12	12.32	0.14
Cloned pUC-P1 in DH5α – intracellular	6.92	48.44	0.50
Cloned pQE-P1 in M15[pREP4] – extracellular	5.50	550.00	6.14
Cloned pQE-P1 in M15[pREP4] – intracellular	212.03	1,484.20	16.20
Cloned pQE-P1 in JM109 – extracellular	2.22	222.00	2.42
Cloned pQE-P1 in JM109 – intracellular	137.84	964.88	10.68

In addition, the expression of the recombinant lipase in *E. coli* M15[pREP4] was induced by the addition of IPTG when the culture grown at 37°C had attained late log phase (OD_{600} of 0.6). The expression was optimized by testing various concentrations of IPTG (0.2, 0.4, 0.6, 0.8, 1, 2, 3, and 5 mM) and various times of induction (1, 2, 3, 4 and 5 h). Expression levels were measured by SDS-PAGE (total

cells lysed by SDS-PAGE sample buffer) and by assaying of lipase activity in cell lysates. The best expression was achieved with 0.4 mM IPTG for 3 h at 37°C showing a bigger band of lipase on SDS-PAGE and the highest activity of lipase (Fig. 3.6).

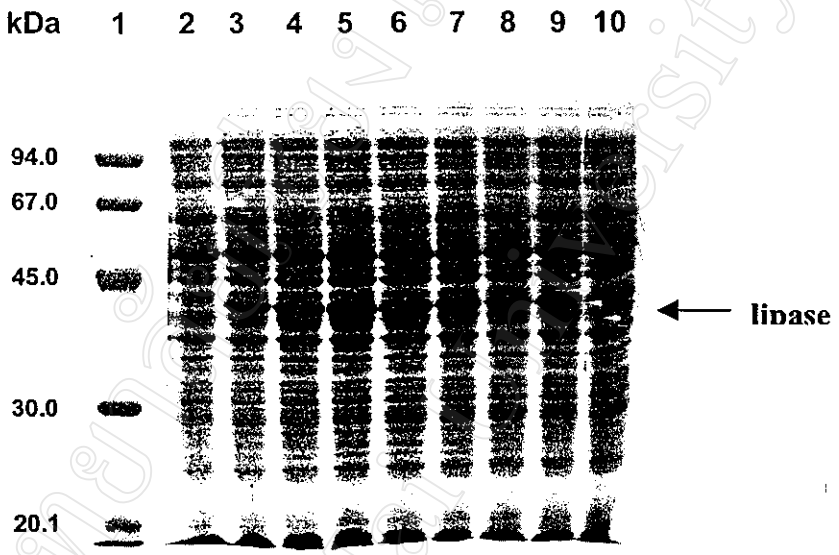

Fig. 3.6. Expression of the cloned lipase from *B. stearothermophilus* P1 by IPTG induction. Lane 1, standard protein markers; and lane 2-10, addition of 0.2, 0.4, 0.6, 0.8, 1, 2, 3, 4, and 5 mM IPTG, respectively.

3.3) Secondary structure prediction and solvent accessibility

The secondary structure prediction and solvent accessibility of the lipase gene were shown in Fig. 3.7. It consisted of α-helix, β-sheet and turns in a different ratio. The hydropathy profile showed the ratio of hydrophilicity and hydrophobicity along the sequence of the lipase. The hydrophilicity of the lipase was slightly more than its hydrophobicity and the non-polar amino acids were slightly less than the polar amino acids in the amino acid composition of the lipase gene structure. In addition, the

surface probability and transmembrane of the lipase gene structure showed the low levels. So, it indicated that in the lipase molecular structure, the non-polar group of amino acid turned into its core structure and the polar group of the amino acid turned outside the molecule.

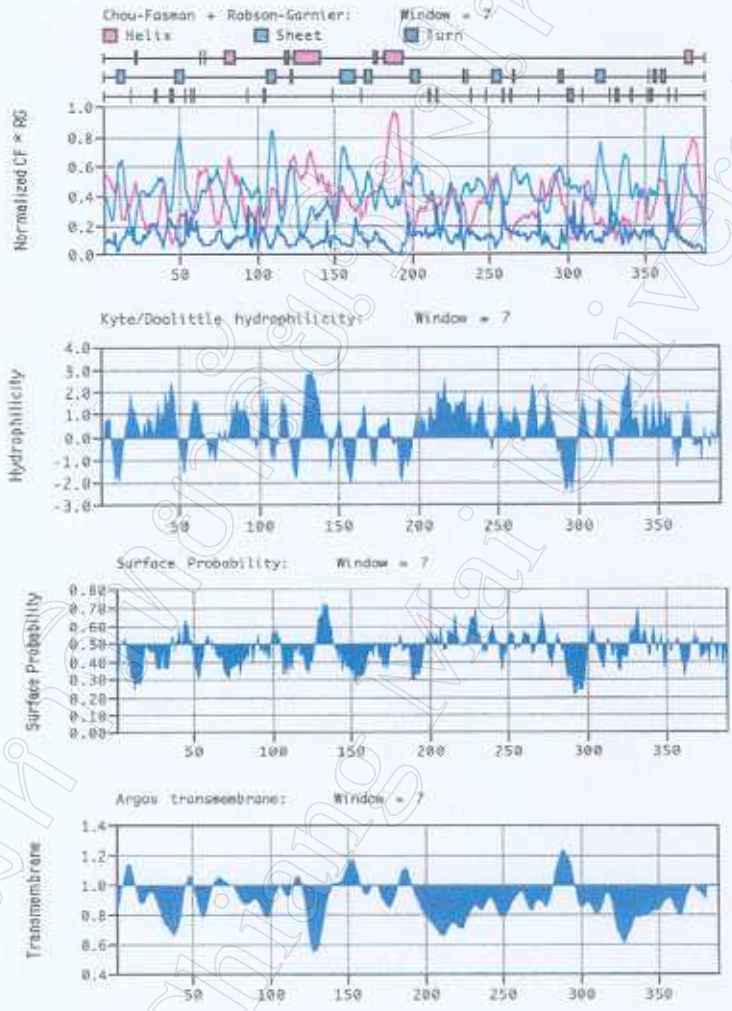

Fig. 3.7. Secondary structure prediction, hydropathy profile, transmembrane and surface probability of a thermostable lipase gene from *B. stearothermophilus* P1. The analysis of the local hydrophilicity and conformational analysis of the lipase structure were based on the methods of Chou and Fishman [75], Garnier *et* al. [76] and Kyte and Doolittle [77].

3.4) Homology modeling and computer graphics of lipase

Results retrieved from the PredictProtein server indicated that 3LIP (*Pseudomonas cepacia*) [93], 1CVL (*Chromobacterium viscosum*) [94], 1OIL (*P. cepacia*) [95] and 1TAH (*P. glumae*) [96], lipases having known 3-D structures appear to have the sequence identity with our model lipase about 40, 55, 40 and 55% identities, respectively. WU-blastp result also showed the sequences of 3LIP, 1CVL, 1OIL and 1TAH producing high-scoring segment pairs with score 68, 54, 68 and 54, respectively. This indicated that the model lipase contained low full-length sequence identity to these reference sequences having known 3-D structures.

Structure alignment (Homology/Insight II) of these references revealed with several structure-conserved regions (SCRs) and the variable regions (VRs) that were mostly on the surface of the protein. Using these alignments, the RMS deviations of the backbone atoms of the structurally conserved regions between the model lipase and the crystal structures of 3LIP, 1CVL, 1OIL and 1TAH were 0.98, 1.08, 1.03 and 1.89 Å, respectively. Otherwise, the major differences between the model lipase and other lipases were on VRs which are the surface loops of varying length. Although the model lipase preserved less sequence similarity in whole to triacylglycerol lipases that have known 3-D structures, the alignment of the model lipase with SCRs of references indicated that it generated much more structure and sequence similarity. Most of SCRs buried in the protein core and the residues with greater RMS located in the outer surface with higher flexibility. Therefore, the sequence alignment of the model lipase to SCRs of references was adopted to be the first step in building model structure.

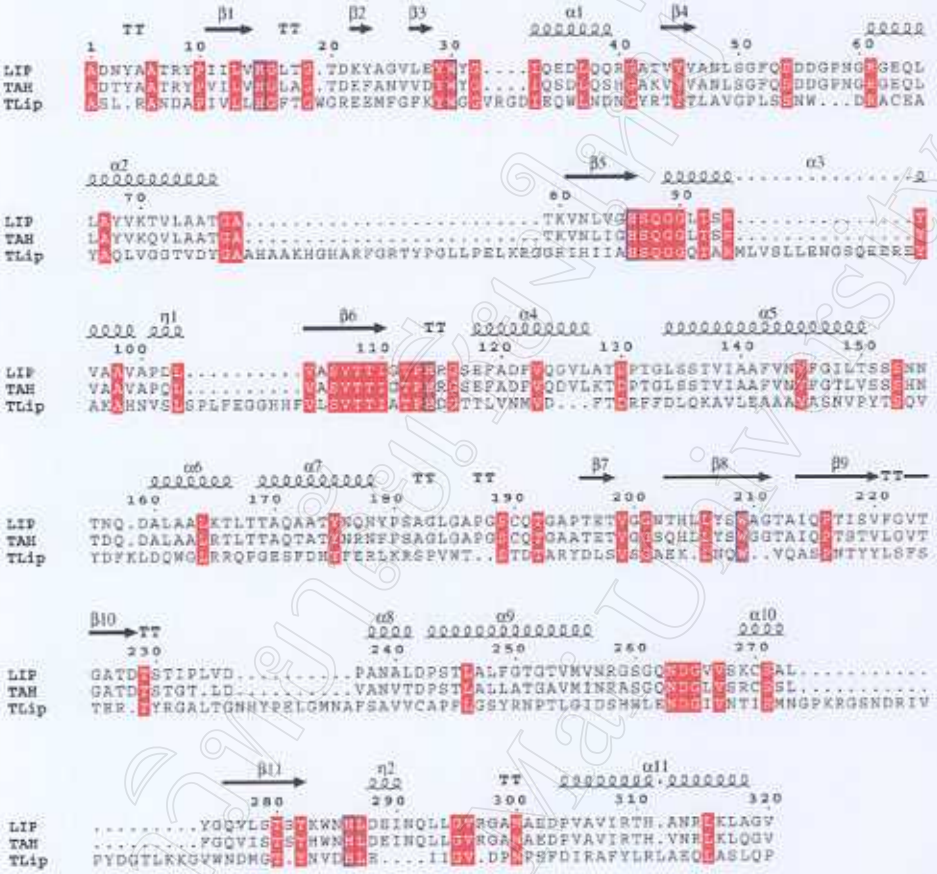

Fig. 3.8. The pair wise alignment of model sequence of *B. stearothermophilus* P1 lipase (TLip) with reference models of lipases from *P. glumae* (1TAH) and *P. cepacia* (3LIP). The red boxes show conserved residues. α, TT and β are helix, turn, and extended sheet, respectively.

(A)

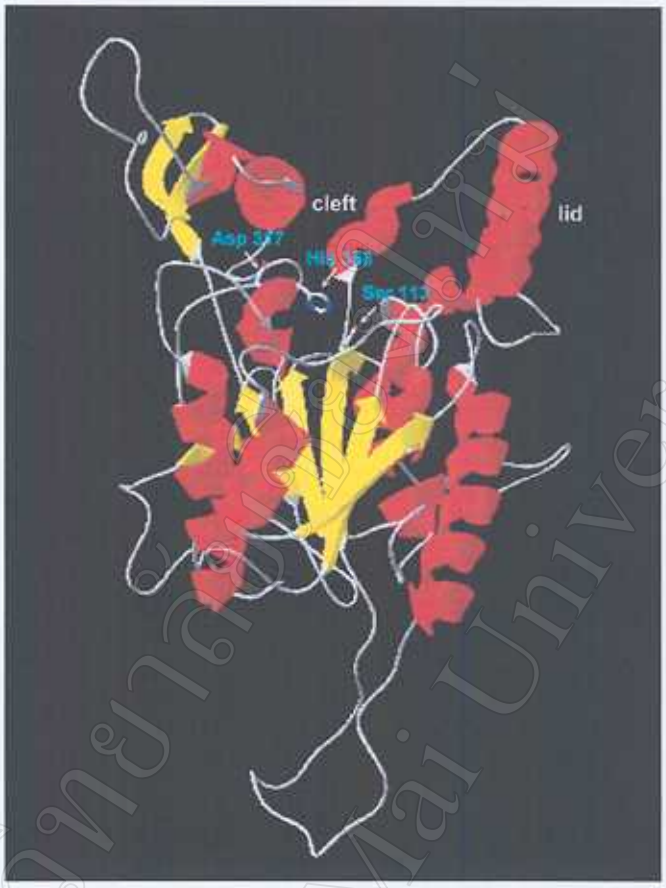

(B)

(C)

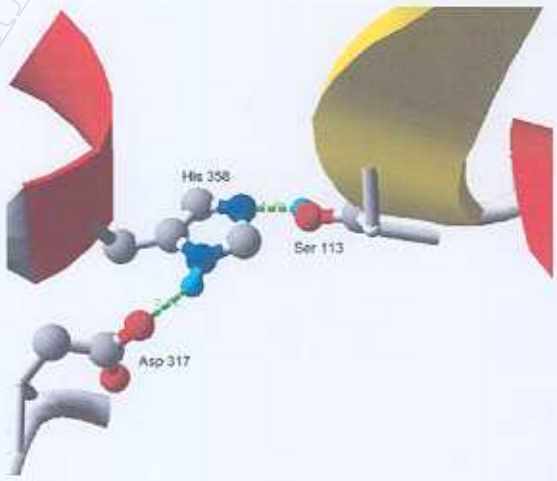

Fig. 3.9. The 3D structures of modeled lipase from *B. stearothermophilus* P1. (A) The modeled structure possess common features of lipase, including both α-helix and extended β-sheet secondary structures in folded protein; the β-sheet was in the core and surrounded by α-helix. (B) The "lid" structure composed by an amphiphilic helix peptide sequence, Phe-180 to Val-197 of the modeled lipase. (C) Ser-113, Asp-317 and His-358 formed the catalytic triad within a range of information H-bond. Color labels: (A) red, helix; yellow, sheet; white, loop; (B) red, non-polar amino acid; green, polar amino acid; blue, acid and basic amino acids; (C) red, oxygen atom; dark blue, nitrogen atom; blue, hydrogen atom; blond, carbon atom; green, strong hydrogen bond.

In study of lipase structure, we used 3LIP as a key reference protein as suggested by MAXHOM showing its 3D homologous structure appeared to have significant sequence identity to the lipase P1 and WU-Blastp result showing higher-score of the sequence producing high-scoring segment pairs. The pair wise alignment of model sequence with reference models, 1TAH and 3LIP, was drawn in the Fig. 3.8. The similar pair wise alignment was input into Modeler (Homology/Insight II) to build initial 3-D models of modeled structure. The predicted model was built by following Homology/Insight II procedure manually and then compared with the reference lipases. The model structure was solvated in water shell and geometry optimized by 2000 steps conjugate gradient energy minimization and showed the force field energies with the total energy of -5267 kcal/mol in 2d4h28m36s, bond of 1046 kcal/mol, angle of 2911 kcal/mol, torsion, 2025 kcal/mol, improper of 1007 kcal/mol and electrostatics of –9816 kcal/mol. The constructed model was overlaid

with 3LIP and 1OIL and shown the RMS deviations to be 1.30 and 1.06 Å with 1132 and 1148 backbone atoms involved, respectively. One of the finally predicted structures was drawn as shown in Fig. 3.9A. Similar to most basic features of lipase, the model structure included both α-helix and extended β-sheet secondary structures in the folded protein and the β-sheet was in the core region surrounding with α-helix. The unique structure feature common to the most lipase was a lid or flap composed by an amphiphilic helix peptide sequence that was posited on the top of the cleft on which bottom sited of the catalytic triad. The helix span between Phe-180 to Val-197 forms the "lid" of the model lipase as shown in Fig. 3.9B. Ser-113, Asp-317 and His-358 were formed the catalytic triad within a range of information H-bond as shown in Fig. 3.9C. The active Ser-113 residue sites on the hairpin turn, where a central β-sheet was converted to α-helix.

3.5) Site-directed mutagenesis

The mutant lipases changing Ser-113, Asp-317 and His-358 to Ala as non-polar amino acid were expressed in *E. coli* M15[pREP4] with the same size of the lipase gene and the same molecular mass of 43 kDa on SDS-PAGE of wild-type (Fig. 3.10). The nucleotide sequences were then determined and found that the position at Ser-113, Asp-317 and His-358 of each mutant were changed to Ala correctly. In addition, the lipase activities of all mutant enzymes decreased significantly 3,441, 2,925 and 3,858-folds of the wide-type enzyme, respectively (Table 3.2). The present work corroborates that this mutant could possibly cause conformational changes of the surrounding residues in the active catalytic center. Therefore, Ser-113, Asp-317

and His-358 are the active site residues of a thermostable lipase from *B. stearothermophilus* P1.

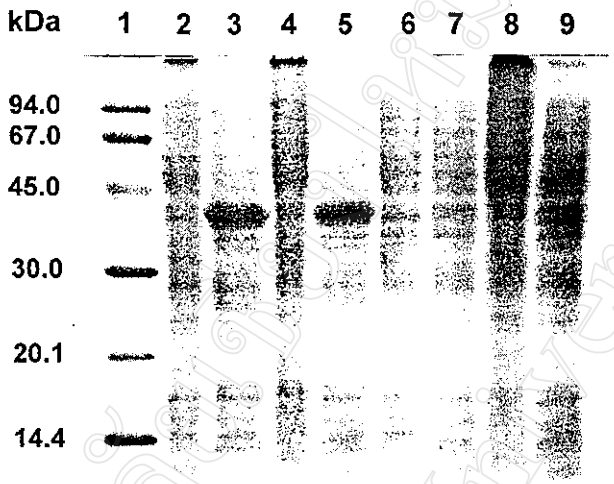

Fig. 3.10. SDS-PAGE shows the induction of cloned lipase P1 (pQE-P1) and its mutants. Lane 1, standard protein marker; Lane 2, pQE-P1 no IPTG; Lane 3, pQE-P1 add IPTG; Lane 4, mutant 1 (Ser-113→Ala) no IPTG; Lane 5, mutant 1 added IPTG; Lane 6, mutant 2 (Asp-317→Ala) no IPTG; Lane 7, mutant 2 added IPTG; Lane 8, mutant 3 (His-358→Ala) no IPTG; Lane 9, mutant 3 added IPTG.

Table 3.2. Comparison of the lipase activities between the pQE-P1 and the mutant lipases.

Recombinant lipase	**Activity (U/ml)**	**Relative activity (%)**
pQE-P1 (control)	208.50×10^3	100
Mutant 1 (Ser-113→Ala)	60.59	0.029
Mutant 2 (Asp-317→Ala)	71.28	0.034
Mutant 3 (His-358→Ala)	54.05	0.026

3.6) Purification of a thermostable lipase

The crude extract obtained by centrifugation of culture broth, sonication, and precipitation with 1% (w/v) streptomycin sulfate was concentrated and partially purified by ultrafiltration using a membrane with a molecular weight cut-off of 10,000 Da. The lipase was partially purified 1.4-fold with 92% yield. The concentrated enzyme was then purified by an ion-exchange chromatographic step with a gradient elution of 1 M NaCl in the basal buffer from a strong anion-exchanger (Q-HyperD^{TM}10) using FPLC (Fig. 3.11). Each fraction was assayed for lipase activity and the lipase pool prepared by selection of fractions with lipase activity. The pooled fractions gave a single band on SDS-PAGE with an apparent molecular mass of approximately 43,652 Da (Fig. 3.12, 3.13). The purity of the purified lipase and its molecular weight of approximately 43,209 Da were confirmed by Mass spectrometer (Fig. 3.14). Both values for the molecular weight agree well with that of 43,203 Da calculated from the deduced amino acid sequence using MacVector sequence analysis software. In addition, the purified lipase was also checked for the purity by HPLC with Nucleosil 7C18 column (4.6×250 mm) and the condition: elution, 0-5-25-30 min = 0-0-100-100%B; flow rate, 1 ml/min; detection, UV 214 nm). It was eluted from the column with 95%B elution and showed a single peak of lipase (Fig. 3.15). The purification procedure was summarized in Table 3.3. The enzyme was purified 18-fold with a yield of 71% from the crude extract.

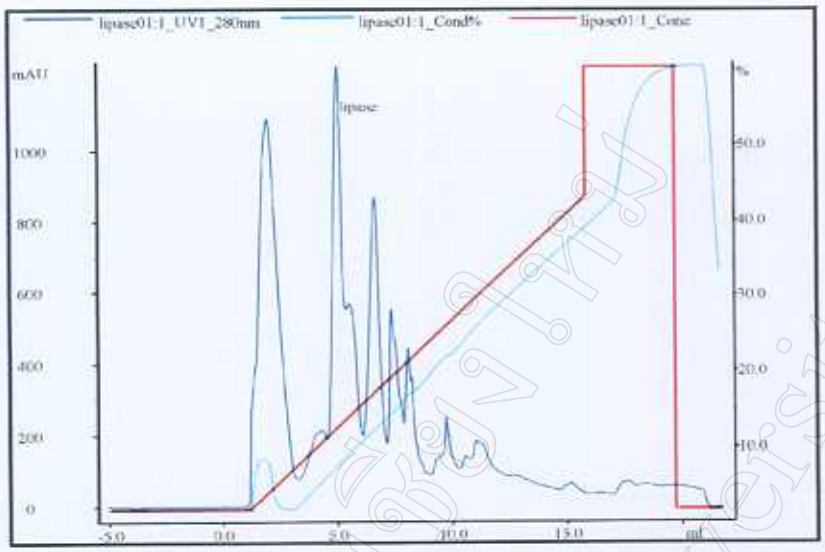

Fig. 3.11. FPLC with Q HyperD anion-exchange chromatography of the purified lipase produced from *B. stearothermophilus* P1. The upper trace shows the absorbance at 280 nm, dark blue line; the conductivity of a linear gradient of 20 mM Tris-HCl buffer pH 7.5 containing 1 M NaCl, light blue line; the concentration of the eluted buffer, red line.

Table 3.3. Summary of the purification of a thermostable lipase from *B. stearothermophilus* P1 (1st procedure).

Step	Volume (ml)	Activity		Protein		Specific activity (U/mg)	Purification fold	Yield (%)
		(U/ml)	Total (U)	(mg/ml)	Total (mg)			
Crude extract	50	1,726	86,300	37.2	1,860	46	1	100
Ultrafiltration	8	9,953	79,620	153.0	1,224	65	1.4	92
Q HyperD column	6	10,275	61,650	12.7	76	811	18	71

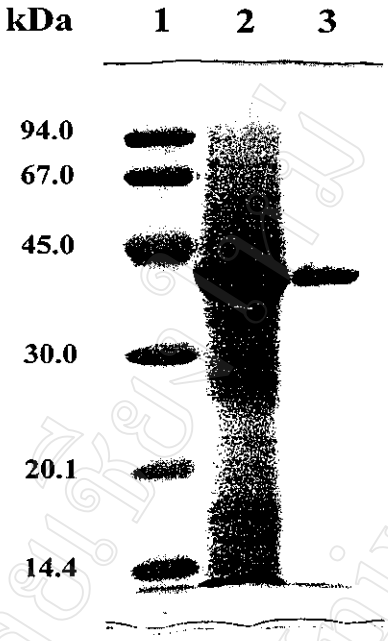

Fig. 3.12. SDS-PAGE of purified lipase from *B. stearothermophilus* P1. Lane 1, molecular weight markers; lane 2, crude extract; lane 3, Q-HyperD^{TM}10-purified lipase.

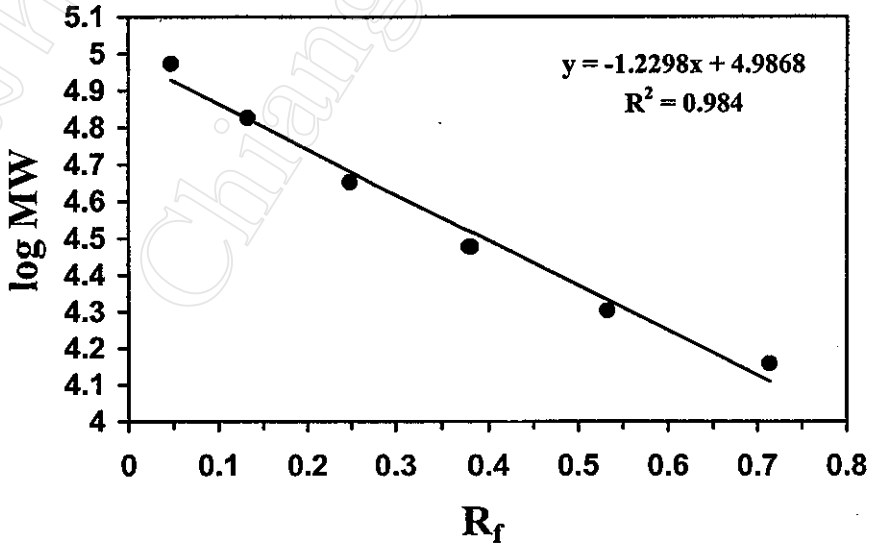

Fig. 3.13. The calibration curve of molecular weight of protein standard by using SDS-PAGE.

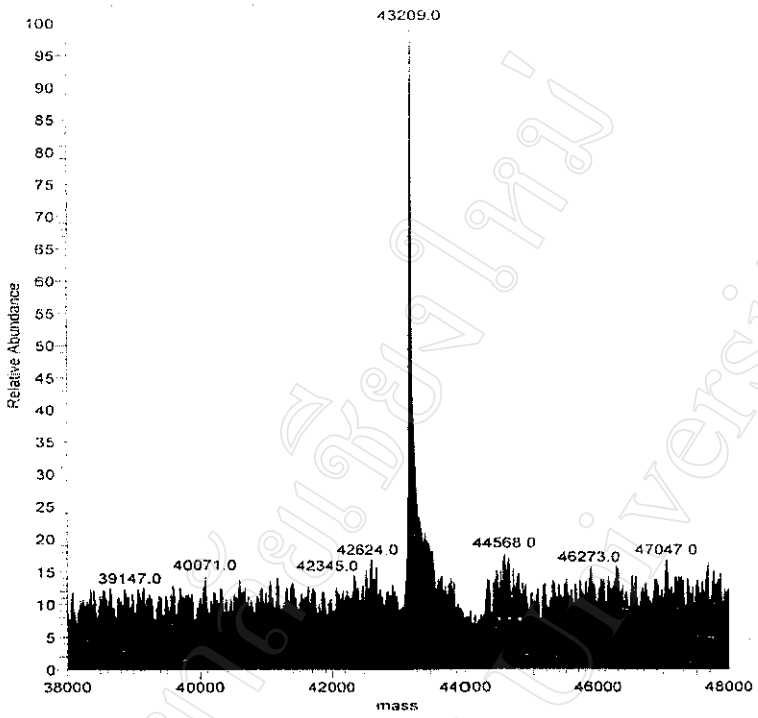

Fig. 3.14. Mass spectrometry of the purified *B. stearothermophilus* P1 lipase.

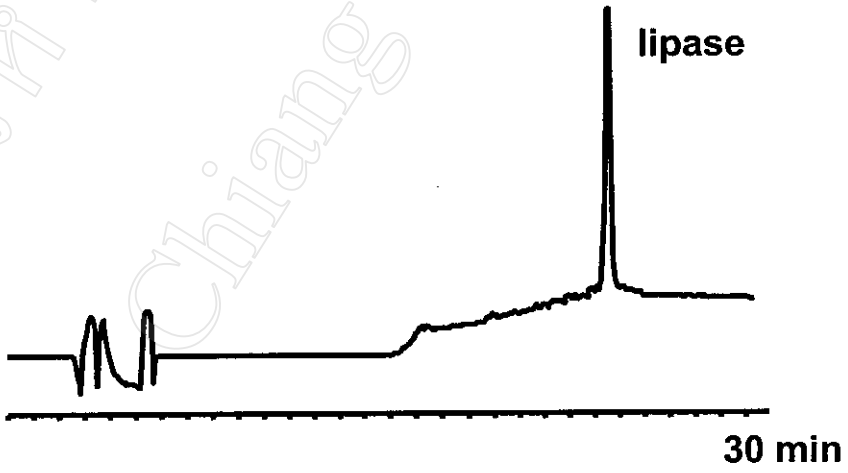

Fig. 3.15. Analysis of the purity of the purified lipase P1 by HPLC. (HPLC condition: column, Nucleosil 7C18 (4.6×250 mm); elution, 0-5-25-30 min = 0-0-100-100%B; flow rate, 1 ml/min; detection, UV 214 nm.)

On the other hand, the purification of the lipase was also done using the other methods that could obtain a higher purity of the purified lipase. Cells were collected from four litres of culture by centrifugation at 6,500 ×g for 30 min and suspended in 50 ml of 20 mM Tris-HCl buffer pH 8.5 containing 10 mM EDTA, 5 mM 3,4-dichloroisocoumarin, 1 mM E64 and 100 mM 1,10-phenanthroline. After sonication, the cell lysate was centrifuged at 12,000 ×g for 30 min and the precipitate discarded. Streptomycin sulphate was added to the supernatant to a final concentration of 1% (w/v) and the precipitate was removed by centrifugation at 12,000 ×g for 15 min. Protein precipitated between 20% saturated and 40% saturated ammonium sulphate was collected by centrifugation at 12,000 ×g for 30 min, and suspended in 20 mM Tris-HCl buffer pH 8.5. The protein was concentrated, desalted and solvent exchanged into the same Tris buffer with a Vivaspin 20 ml centrifugal concentrator (Vivasciences) with a molecular weight cut-off of 10,000. The concentrated lipase was then purified by perfusion chromatography with Poros 20 HQ column (4.6 x 100 mm) using a BioCAD workstation (Applied Biosystems) (Fig. 3.16). The largest peak (eluting at 0.18 M NaCl) contained high lipase activity and the corresponding fractions were pooled and concentrated with a Vivaspin tube. It was then purified by gel filtration on Sephacryl S-200 column and a single peak of lipase activity was obtained (Fig. 3.17). The fractions with high lipase activity were pooled and the purity was checked by SDS-PAGE (Fig. 3.18). The purified lipase showed a single band by SDS-PAGE and was purified 39-fold over the crude extract with a yield of 19% (Table 3.4). The molecular mass of the purified lipase was shown to be 43 kDa by SDS-PAGE and mass spectrometry.

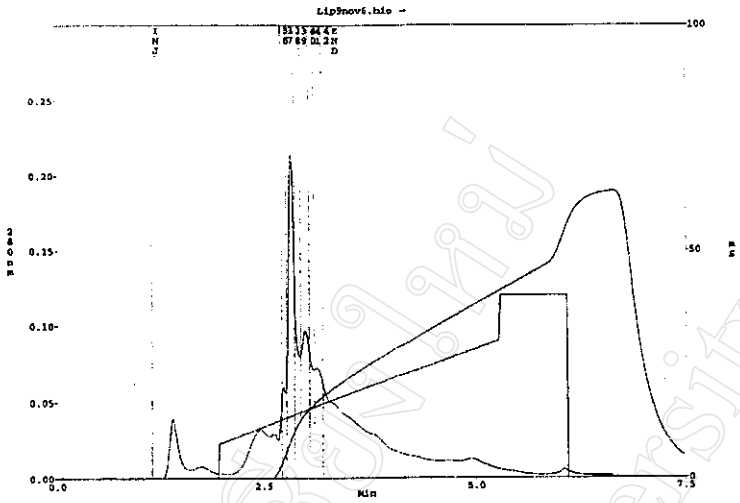

Fig. 3.16. Purification of the lipase by perfusion chromatography with Poros 20 HQ column (4.6 x 100 mm) using a BioCAD workstation. Elution was with 20 mM Tris-HCl buffer pH 8.5 containing a linear gradient of 0.15 to 0.6 M NaCl at a flow rate of 10 ml.min^{-1}. The separate traces indicate the absorbance at 280 nm, the NaCl gradient and the conductivity.

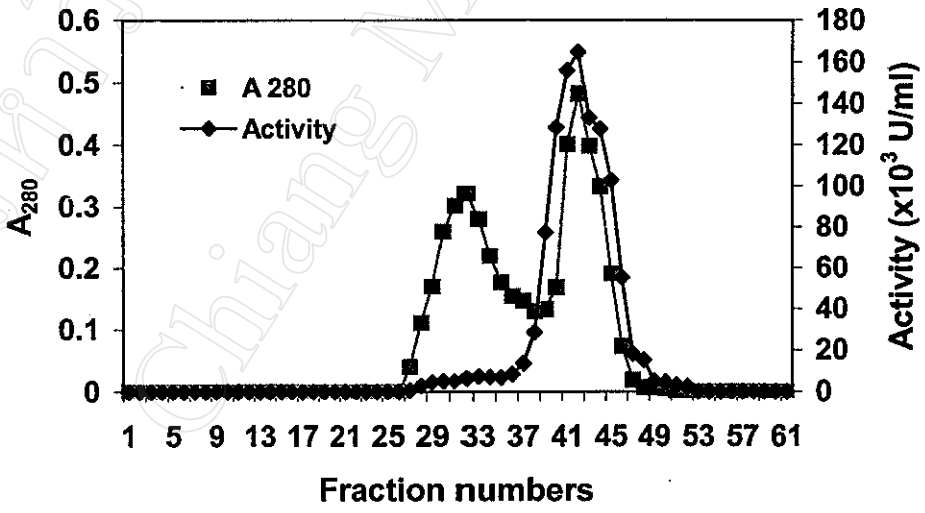

Fig. 3.17. Purification of the lipase by gel filtration chromatography with Sephacryl S-200HR column (1.6×100 cm). The column was eluted with 20 mM Tris-HCl buffer pH 8.5 at a flow rate of 0.25 ml/min. Symbols; ●, lipase activity; and ■, squares, A280 nm.

Table 3.4. Summary of the purification of a thermostable lipase from *B. stearothermophilus* P1 (2nd procedure).

Step	Volume (ml)	Activity		Protein		Specific activity (U/mg)	Purification Fold	Yield (%)
		(U/ml)	Total (U)	(mg/ml)	Total (mg)			
Crude extract	11.8	3,459	40,643	52.0	611	66.5	1.00	100
20-40% $(NH_4)_2SO_4$ precipitation	5.5	5,514	30,327	24.0	132	230	3.45	74.6
HQ column	14.0	872	12,208	1.04	14.6	836	12.6	30.0
Sephacryl S-200HR	8.7	897	7,804	0.35	3.0	2,601	39.1	19.2

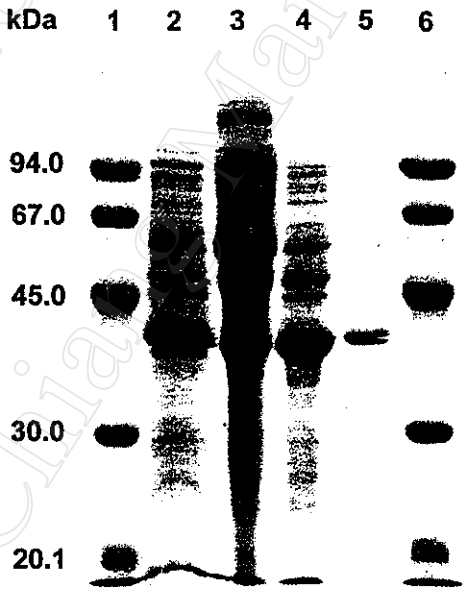

Fig. 3.18. SDS-PAGE of purified lipase from *B. stearothermophilus* P1. Lane 1 and 6, molecular weight markers; lane 2, crude extract; lane 3, 20-40% saturated ammonium sulphate precipitate; lane 4, Poros HQ purified lipase; lane 5, Sephacryl S-200HR purified lipase.

3.7) Characterization of the purified lipase

3.7.1) Effect of pH on the lipase activity and stability

The effect of pH on lipase activity at 55°C with *p*-NP caprate as substrate was examined at various pH values. The enzyme was active in the pH range 7.5-10.0 and the optimal pH was shown to be 8.5 in 50 mM Tris-HCl buffer (Fig. 3.19A). Consistently higher activity was observed with the Tris-HCl buffer than with sodium acetate, phosphate and Tris-glycine buffer. At 55°C, the lipase was stable for 1 h in a wide range of buffers between pH 8.0-11.0 (Fig. 3.19B). It showed greatest stability at pH 8.5-9.0 that was the same range as the optimal pH.

3.7.2) Effect of temperature on the lipase activity and stability

To test the effect of temperature on lipase activity, assays were performed for 1 h at various temperatures. The lipase was most active in the temperature range 45-65°C, with maximal activity at 55°C (Fig. 3.20A). The thermostability of the enzyme was examined by measuring the residual activity at different times of incubation for up to 15 h at various temperatures at pH 8.5. After incubation for 1 h, the enzyme was stable at 30-65°C with a residual activity greater than 50% of the initial activity (Fig. 3.20B). At 55°C, the optimal temperature for activity, it was stable for more than 6 h and had a half-life of about 7.6 h. Prolonged incubation at all temperatures resulted in loss of activity.

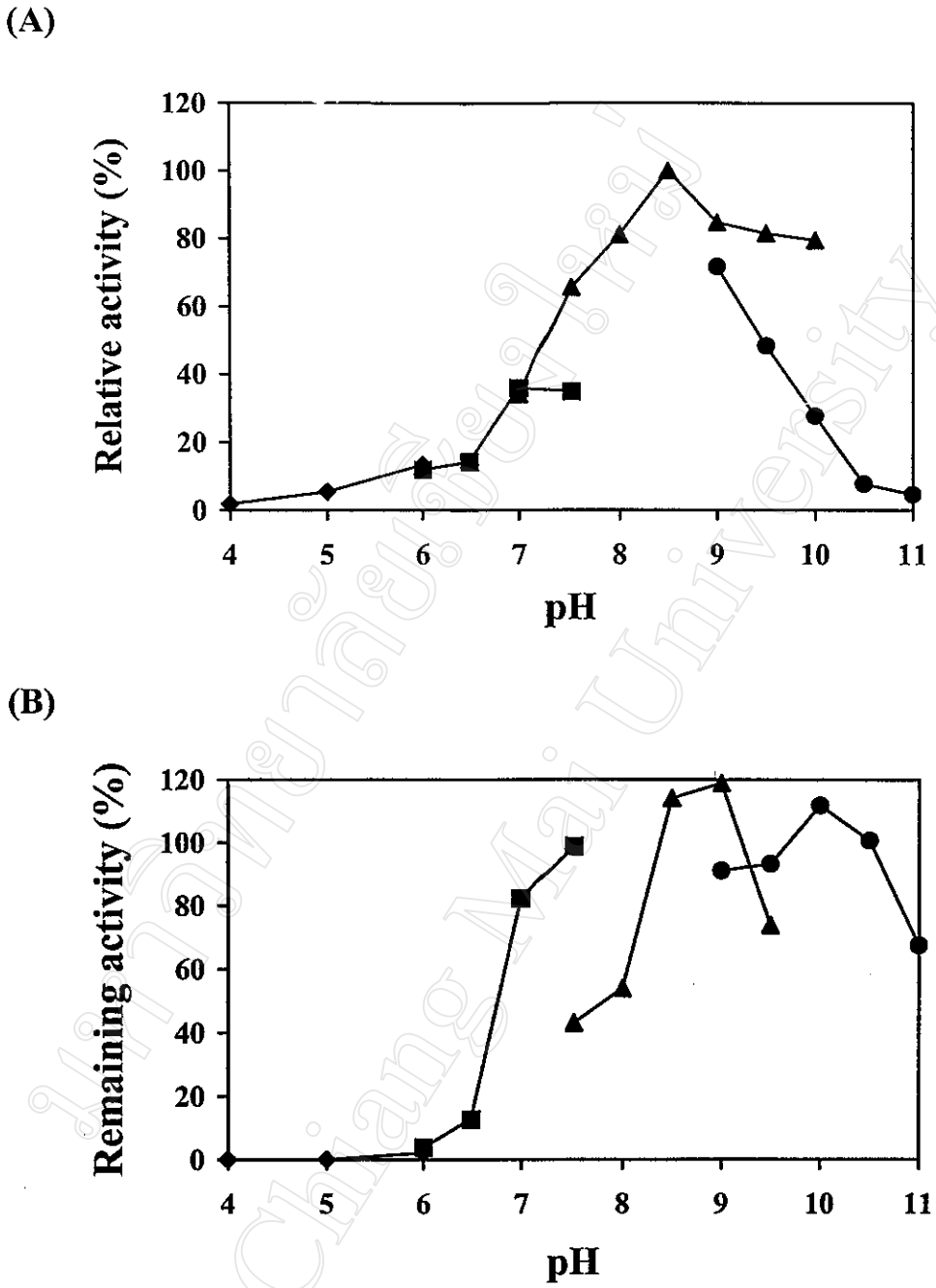

Fig. 3.19. Effect of pH on lipase activity (A) and stability (B). A: The purified lipase was assayed in various pH buffers, as described in the text. B: The purified lipase was incubated in various pH buffers for 1 h at 55°C, then assayed in the normal way. Symbols: ♦, Sodium acetate buffer; ■, Phosphate buffer; ▲, Tris-HCl buffer; ●, Tris-glycine buffer.

(A)

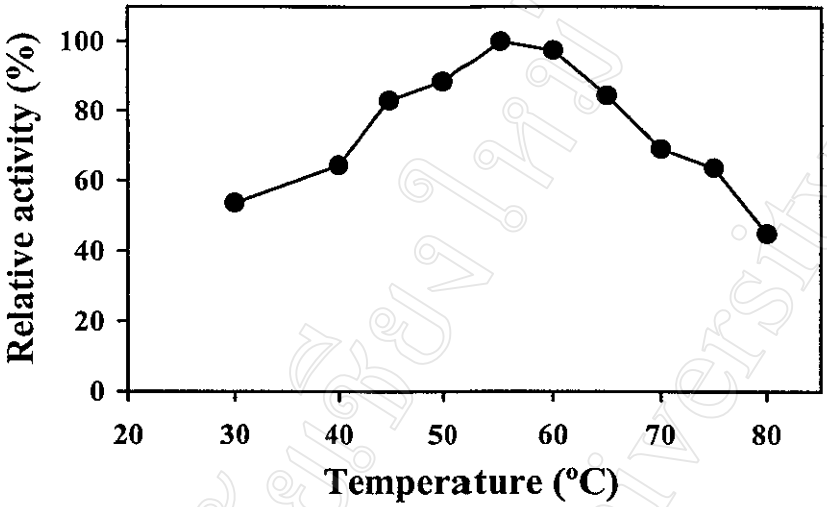

(B)

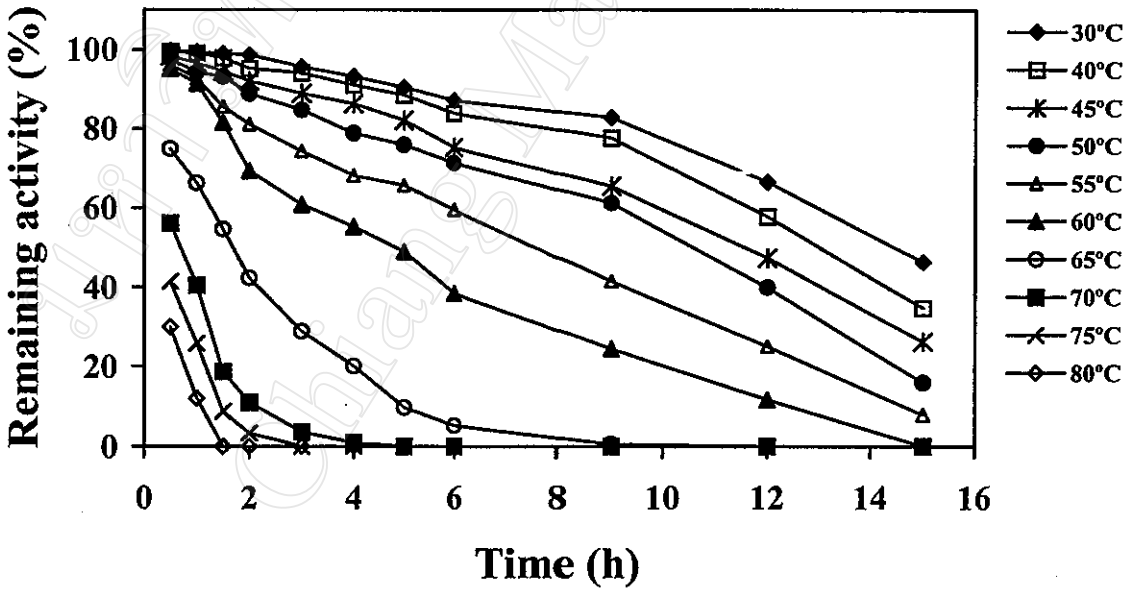

Fig. 3.20. Effect of temperature on lipase activity and stability. A: The effect of temperature on lipase activity was determined at various temperatures, as described in the text. B: The effect of temperature on lipase stability was determined by incubating the pure lipase at various temperatures for up to 15 h and measured the remaining activity.

3.7.3) Substrate specificity

The lipase hydrolyzed synthetic substrates with acyl group chain lengths of between C8 and C12, with optimal activity with C10 (*p*-NP caprate) (Fig. 3.21). The lipase activity on long-chain of substrates was between 70-100% of optimal for C8 or C10 groups and 30-50% for C12 to C18, whereas, with short-chain substrates (C2-C6), lipase activity was less than 30%. In addition, the lipase hydrolyzed triacylglycerols with acyl group chain lengths of between C8-C12, with optimal activity with C8 (tricaprylin). Moreover, the lipase hydrolyzed trilinolenin more than trilinolein and triolein.

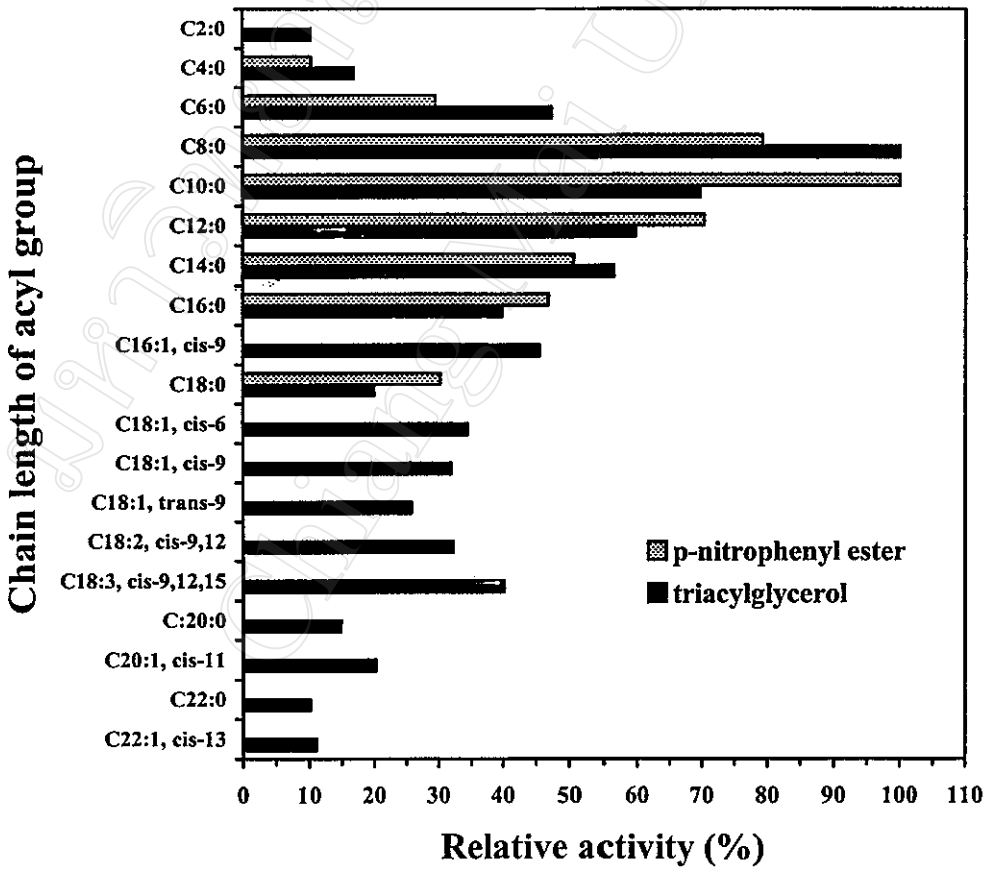

Fig. 3.21. Substrate specificity of the lipase using several *p*-NP esters and triacylglycerols.

3.7.4) Study of the kinetic parameters (K_m and V_{max}) of the lipase

The kinetic parameters of the lipase could be determined by using Michaelis-Menten equation and Lineweaver-Burk plot. The rate of reactions was observed by using *p*-NP caprate as the substrate in various concentrations of 0.2-5 mM and showed in Table 3.5. The result of the initial rate and concentrations of substrate could be used to plot a graph to determine the Michaelis constant (K_m) as shown in Fig. 3.22 and the Lineweaver-Burk between 1/[S] and 1/[V_i] for determination of the Michaelis constant, K_m and V_{max}, was shown in Fig. 3.23. The K_m and V_{max} values at 55°C were found to be 0.286 mM and 88 $U.ml^{-1}min^{-1}$, respectively.

Table 3.5. The initial velocity (V_i) of the enzyme reaction using various substrate concentrations (S).

S (mM)	V_i ($\times 10^3$U/ml/min)	1/S (1/mM)	$1/V_i$ (min/ml/$\times 10^3$U)
0.2	0.0350	5.00	28.57
0.4	0.0500	2.50	20.00
0.6	0.0611	1.67	16.37
0.8	0.0667	1.25	14.99
1.0	0.0700	1.00	14.29
2.0	0.0750	0.50	13.33
3.0	0.0769	0.33	13.00
5.0	0.0778	0.20	12.85

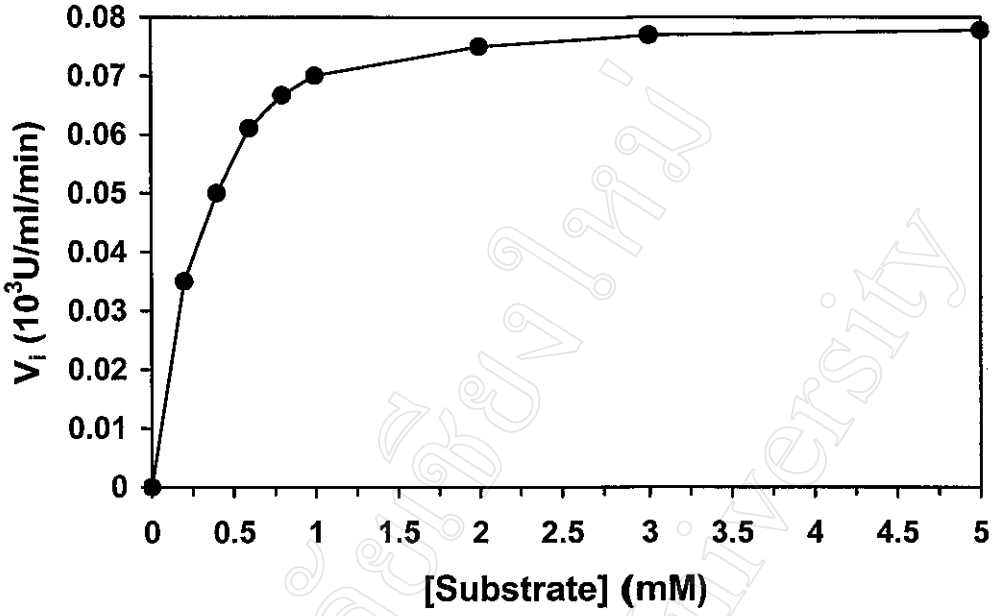

Fig. 3.22. Michaelis-Menten type plot of lipase hydrolysis rate at different concentrations of *p*-NP caprate.

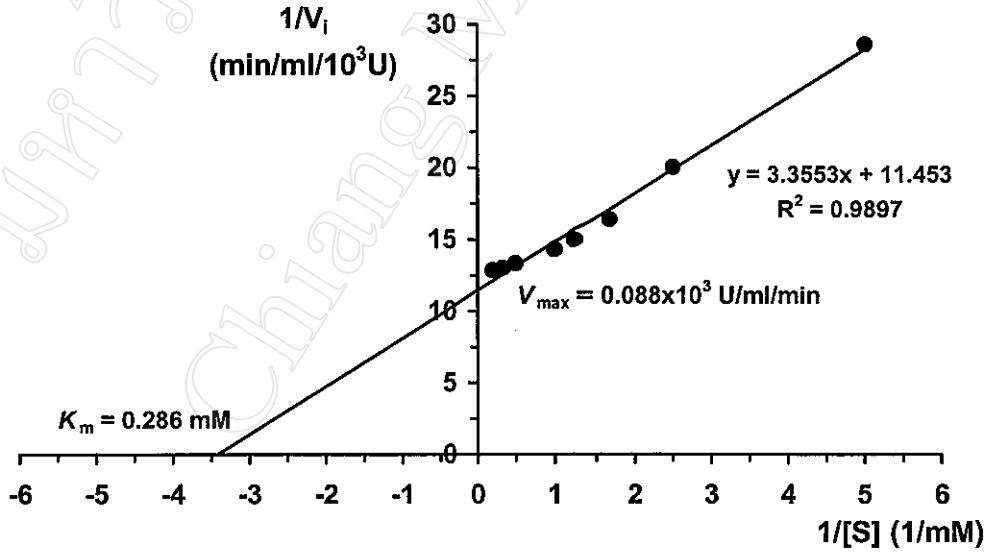

Fig. 3.23. Lineweaver-Burk plot between 1/initial velocity of reaction versus 1/ concentrations of *p*-NP caprate.

3.7.5) Positional specificity

All substrates; 1-mono-, 1,2-di-, 1,3-di- and triolein, were hydrolyzed by the lipase. At 55°C, the acyl migration was occurred, which could be seen in the control (without enzyme) but containing 1,2- and 1,3-diolein substrate solutions, respectively. After 1 h of incubation, more oleic acid was released from 1,3-diolein as confirmed by running TLC (Fig. 3.24). The lipase activity was also checked and found that their activities for the hydrolysis of monoolein, 1,2-diolein, 1,3-diolein and triolein were 7.96, 3.54, 2.39 and 6.80 U/ml, respectively.

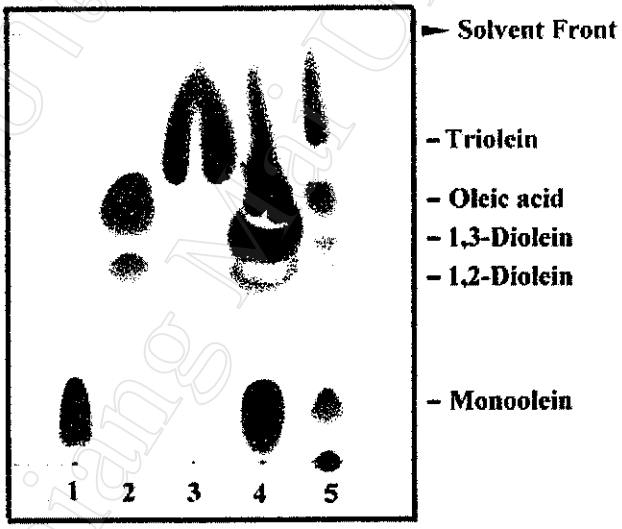

Fig. 3.24. Thin layer chromatography of the hydrolysis of the cloned lipase P1 on triolein substrates. Spots were developed with iodine vapor. Symbols: 1, monoolein; 2, 1,2 diolein & 1,3 diolein; 3, triolein, mixture of mono, di- and triolein; 4, the hydrolysis of lipase on the mono-, di- and triolein mixtures.

3.7.6) Effect of metal ions on the lipase activity

The effect of metal ions was tested for studying the influence of metal ions on the activity of lipase including the determination of metal ions that can activate the activity of lipase. In the presence of 1 mM of most tested metal ions, activity was decreased slightly; however, $ZnCl_2$ and $FeSO_4$ reduced the lipase activity to 35% and 53%, respectively (Table 3.6). Using 10 mM metal ions, the inhibitory effects were greater, and $ZnCl_2$ and $FeSO_4$ (10 mM) caused almost complete block of lipase activity and the activities were remained about 1.6 and 0.76%, respectiveiy.

Table 3.6. Effect of metal ions on the purified lipase. The lipase was pre-incubated at room temperature with various metal ions at concentrations of 1 and 10 mM and then the activities were assayed.

Metal ions	Concentration (mM)	Relative activity (%)
Control	0	100
$CaCl_2$	1	96
	10	92
$CuCl_2$	1	84
	10	63
$MgCl_2$	1	98
	10	90
$MnCl_2$	1	84
	10	41
$ZnCl_2$	1	35
	10	2
CsCl	1	90
	10	84
KCl	1	87
	10	72
LiCl	1	84
	10	71
NaCl	1	97
	10	90
$FeSO_4$	1	53
	10	1

3.7.7) Effect of inhibitors on the lipase activity

The effect of various inhibitors on lipase activity is shown in Table 3.7. All inhibitors were effective at 10 mM. Significant inhibition was already observed at 5 min and the inhibition increasing depending on the time of incubation. The chelating agent EDTA did not have high effect on the activity of the lipase, and this suggested that it was not a metalloenzyme. The lipase was strongly inhibited by the addition of 10 mM PMSF (77% inhibition) or 1-hexadecanesulfonyl chloride (93% inhibition), showing that a serine residue plays a key role in the catalytic mechanism. After 10 min incubation, the activities of lipases with PMSF, 1-dodecanesulfonyl chloride and 1-hexadecanesulfonyl chloride were significant decreased; especially 1-hexadecanesulfonyl chloride completely abolished the activity of lipase.

Table 3.7. Effect of inhibitors on the purified lipase. The lipase was incubated with each inhibitor in the final concentration of 10 mM at 37°C for 5, 10 and 30 min and then the remaining activities were assayed.

Inhibitors	**Remaining activity (%)**		
	5 min	**10 min**	**30 min**
Control	100	97	95
DTT	83	79	74
EDTA	76	73	69
β-mercaptoethanol	88	87	80
PMSF	23	11	2
1-Dodecanesulfonyl chloride	42	20	5
1-Hexadecanesulfonyl chloride	7	0	0

3.7.8) Effect of detergents on the lipase stability

On the addition of 0.1% (w/v) detergents, no effect on lipase activity was seen except in the case of SDS, sodium deoxycholate and Tween 20 which slightly reduced activity (Table 3.8). At 1% detergent, a greater effect was seen, especially with SDS, which reduced the activity about 50% and Tween 20 which strongly inhibited lipase activity. After incubation in the presence of 0.1% detergent at 37°C for 1 h, CHAPS and Triton X-100 increased enzyme stability whereas SDS, sodium deoxycholate and Tween 20 decreased the stability; in the presence of 1% detergents, the activity was decreased more than 50% except in the case of CHAPS and Triton X-100.

Table 3.8. Effect of detergents on the purified lipase. The lipase was incubated at 37°C for 1 h in 20 mM Tris-HCl buffer pH 8.5 with detergents.

Detergents	**Concentration (%, w/v)**	**Relative activity (%)**	
		0 h	**1 h**
Control	0	100	82
CHAPS	0.1	100	91
	1.0	72	58
SDS	0.1	80	57
	1.0	57	37
Sodium deoxycholate	0.1	95	67
	1.0	71	42
Triton X-100	0.1	101	96
	1.0	74	50
Tween 20	0.1	95	68
	1.0	20	14

Table 3.9. Effect of organic solvents on the purified lipase. The lipase was incubated at 37°C for 30 min in several organic solvents and then the residual activities were assayed.

Organic solvents	**log P***	**Relative activity (%)**	
		0 min	**1 h**
Control	-	100	97
Methanol	-0.77	83	45
Acetonitrile	-0.34	66	0.2
Ethanol	-0.32	79	66
Acetone	-0.24	72	78
Iso-propanol	0.05	52	39
Butanol	0.88	77	14
Diethyl ether	0.89	85	67
Dichloromethane	1.25	86	74
Benzene	2.00	90	92
Chloroform	2.24	92	92
Toluene	2.69	88	93
Cyclohexane	3.44	70	46
Hexane	3.48	61	54
n-Heptane	4.00	88	95
Iso-octane	4.52	69	60

*The logarithm of the solvent partition coefficient between octanol and water.

3.7.9) Effect of organic solvents on the lipase stability

After the enzyme was incubated in the presence of 30%v/v organic solvents at 37°C for 1 h, it was found that the enzyme could be stable in the presence of ethanol, acetone, diethyl ether, dichloromethane, benzene, chloroform, toluene, hexane, n-

heptane and iso-octane (Table 3.9). It was highly stable in the presence of n-heptane, toluene, benzene and chloroform but it was inactive in the presence of acetonitrile and butanol. Otherwise, its thermostability did not depend on the log P of organic solvents.

3.7.10) Crystallization of the lipase

The purified lipase P1 was crystallized by using hanging drop technique. The crystals of lipase P1 grew rapidly after 24 h at 16°C (289 K) and the crystallization conditions were 20% saturated ammonium sulphate as precipitants and a droplet containing 15 $mg.ml^{-1}$ of protein in the buffer of 0.1 M Hepes pH 6.8-7.0. The size of the crystal was 0.2 mm by 0.35 mm by 0.35 mm and had the tetragonal shape as shown in Fig. 3.25.

Data were collected to 2.5 Å at the ESRF facility (λ = 0.931 Å), Grenoble. Data were processed using DENZO and Scalepack (Otwinowski & Minor, 1997). The statistics are presented in Table 3.10. There is one molecule per asymmetric unit [Vm = 2.92 01 $Å^3$ Da^{-1} (Matthews, 1968)].

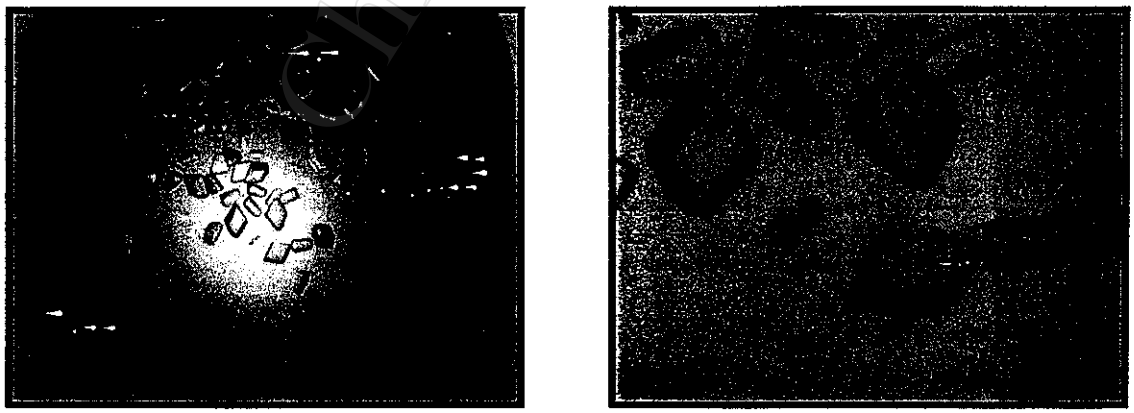

Fig. 3.25. Crystallization of the thermostable lipase from *B. stearothermophilus* P1.

Table 3.10. Crystallographic statistics for *B. stearothermophilus* P1 lipase.

Resolution (Å)	30.0-2.5
Space group	C2
a (Å)	117.54
b (Å)	80.82
c (Å)	99.36
β (°)	96.35
R_{merge}	0.109
(Top shell)	0.401
Completeness %	94.3
(Top shell)	88.6
Number of observations	89044
Number of reflections	30531

3.7.11) Comparison of the lipase structure from structural modeling and X-ray crystallography

From the lipase crystals, the lipase structure was determined by using soaking technique with the metal ions such as Cu or Zn. The result showed that the overall structure obtained from X-ray crystallography was similar to the modeled lipase and the other lipases that were alpha/beta fold with a lid (Fig. 3.26). The catalytic site was Ser-113, Asp-317 and His-358. There was a calcium ion near the active site in the monomer. The residues surrounding that ion were His81 and His87, Asp61 and Asp238. The calcium ion was surrounded by Gly286 O, Glu360 Oe2, Asp365 Od1, Pro366 O and a water.

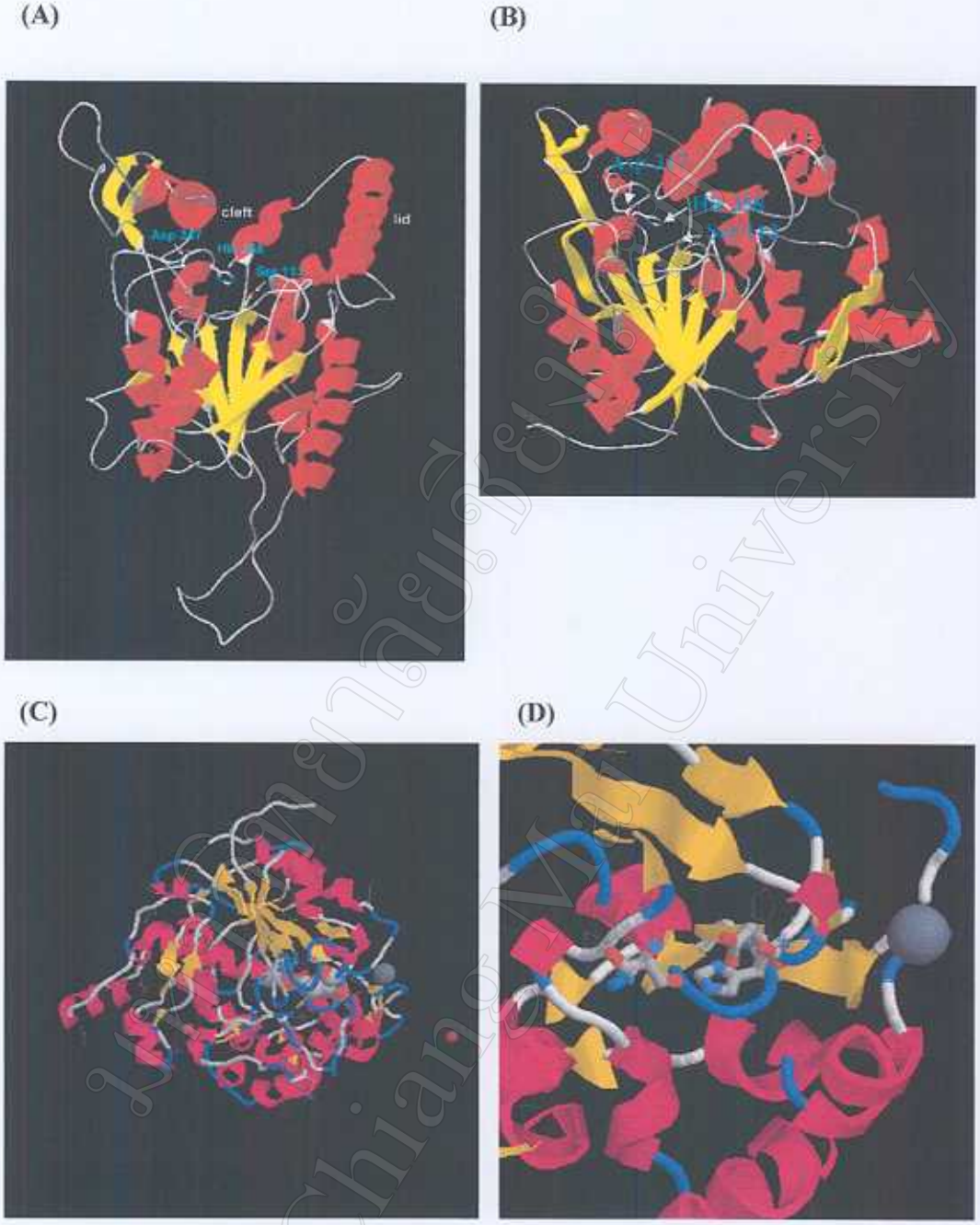

Fig. 3.26. Comparison of the lipase structure from the structural modeling (A) and X-ray crystallography (B, C, D).

3.8) Chiral separation of lipase

The lipase P1 catalyzed the acylation of diol-substrate, 3-phenoxy-1,2-propanediol to form the first product, 1-acetyl-3-phenoxy-1,2-propanediol or 2-acetyl-3-phenoxy-1,2- propanediol and then the second product, 1,2-diacetyl-3-phenoxy-1,2-propanediol. The unreacted starting material of 3-phenoxy-1,2-propanediol was analyzed by Chiral OD-RH column. R(+) 3-Phenoxy-1,2-propanediol was eluted at the retention time of 4.776 min and the S(–) 3-phenoxy-1,2-propanediol was eluted at the retention time of 5.221 min (Fig. 3.27). The lipase P1-catalyzed acetylation has the enantiomeric preference of S(–) 3-phenoxy-1,2- propanediol when the reaction was performed in acetone, chloroform, and dichloromethane. The ratio of unreacted substrate R(+)/S(–) in acetone and chloroform is 2:1 whereas the ratio in dichloromethane is 3:1.

In addition, the comparison of the reaction between 3-phenoxy-1,2-propanediol and lipase in different organic solvents such as acetone, dichloromethane and chloroform (log P = -0.24, 1.25 and 2.24, respectively) and temperatures (room temperature and 55°C) showed that the lipase catalyzed acetylation in dichloromethane better than in acetone and chloroform and its reaction was happened rapidly less than 0.5 h (Fig. 3.28, 3.29, 3.30). Otherwise, the reactions at 55°C were faster than at room temperature. Otherwise, when the enantioselectivity of the lipase from *B. stearothermophilus* P1 on 3-phenoxy-1,2-propanediol in dichloromethane at 55°C for 1 h was compared to the other lipases, the result showed that the lipase P1 catalyzed the acetylation of 3-phenoxy-1,2-propanediol better than the other lipases except the lipase from *Candida* sp. and *Geotrichum candidum* (Fig. 3.31).

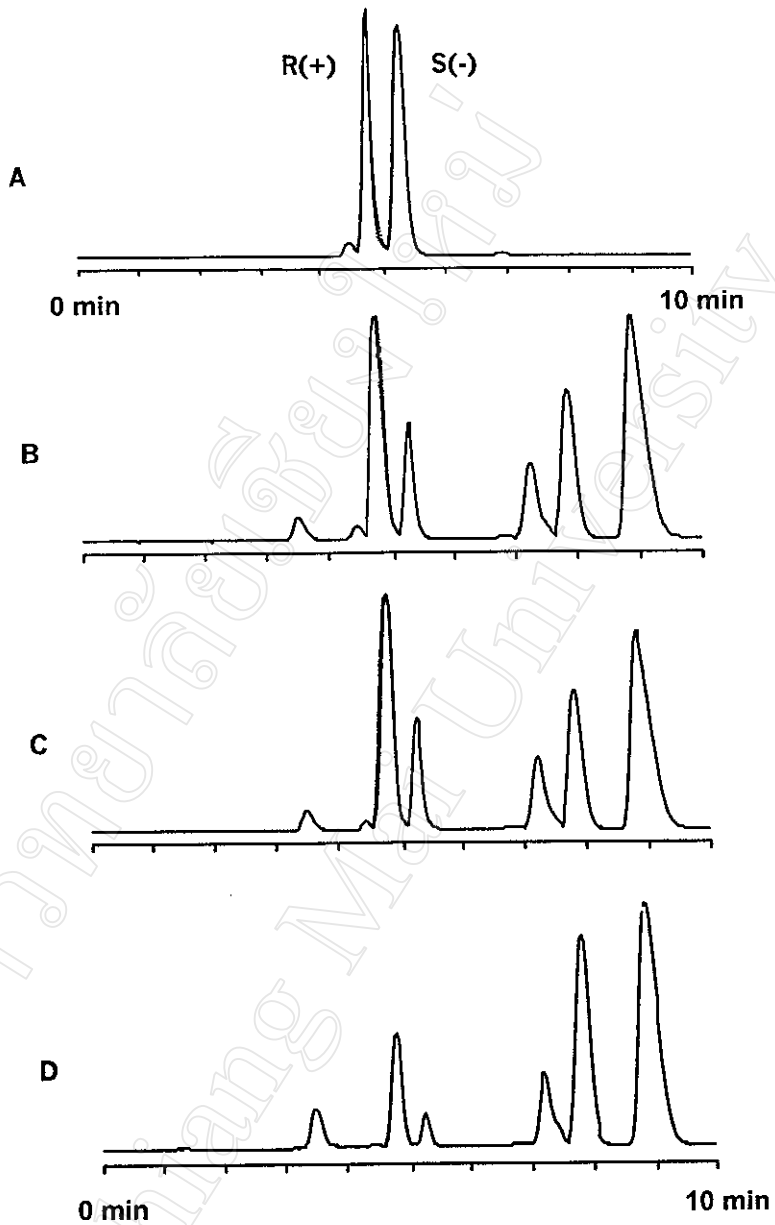

Fig. 3.27. Analysis of unreacted starting material of 3-phenoxy-1,2-propanediol catalyzed with lipase from *B. stearothermophilus* P1 by Chiralcel OD-RH. A, standard 3-phenoxy-1,2-propanediol; B, reaction in acetone; C, reaction in chloroform; D, reaction in dichloromethane.

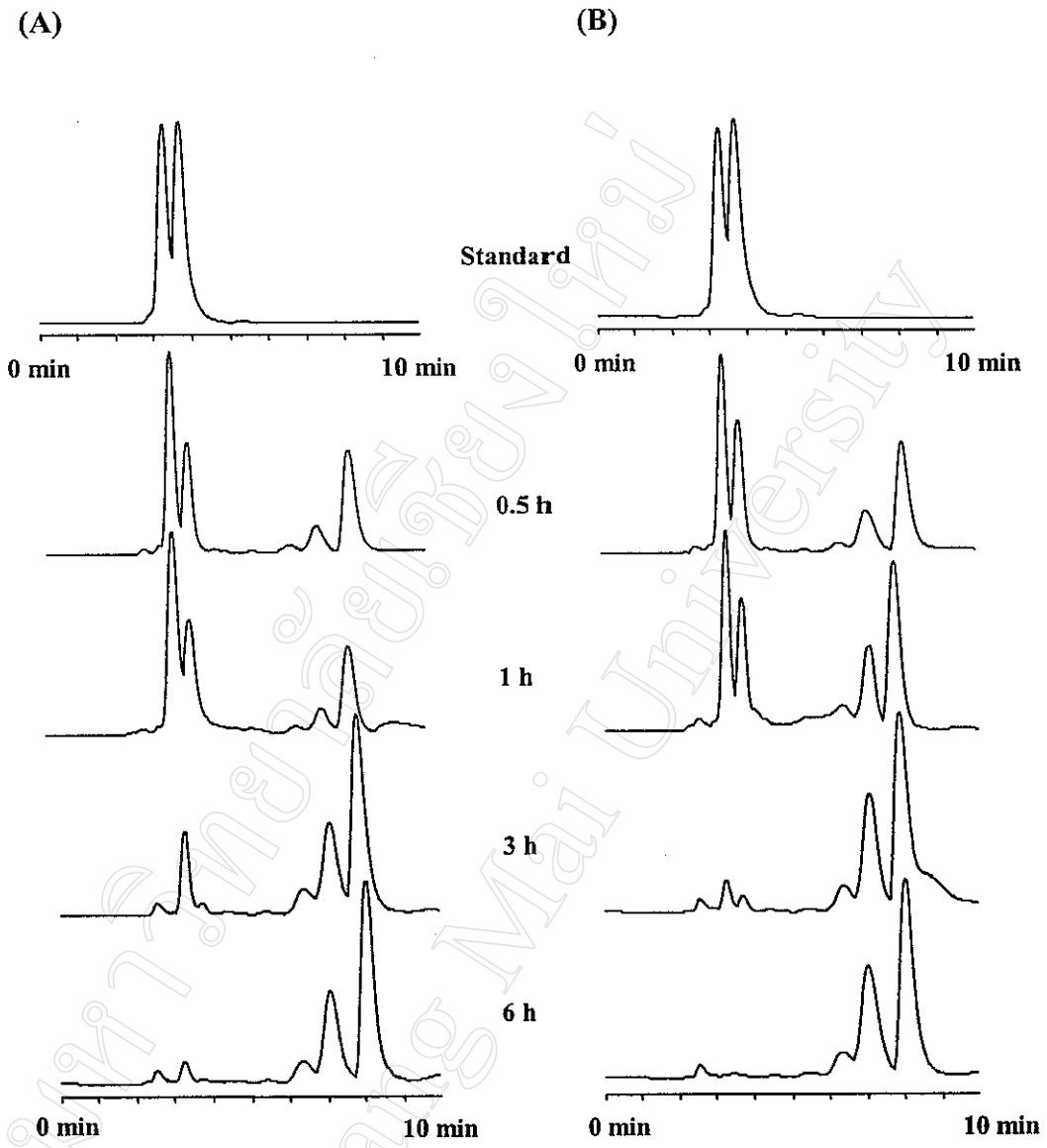

Fig. 3.28. Analysis of unreacted starting material of 3-phenoxy-1,2-propanediol catalyzed with lipase from *B. stearothermophilus* P1 in acetone at room temperature (A) and 55°C (B) for 0.5, 1, 3 and 6 h by Chiralcel OD-RH.

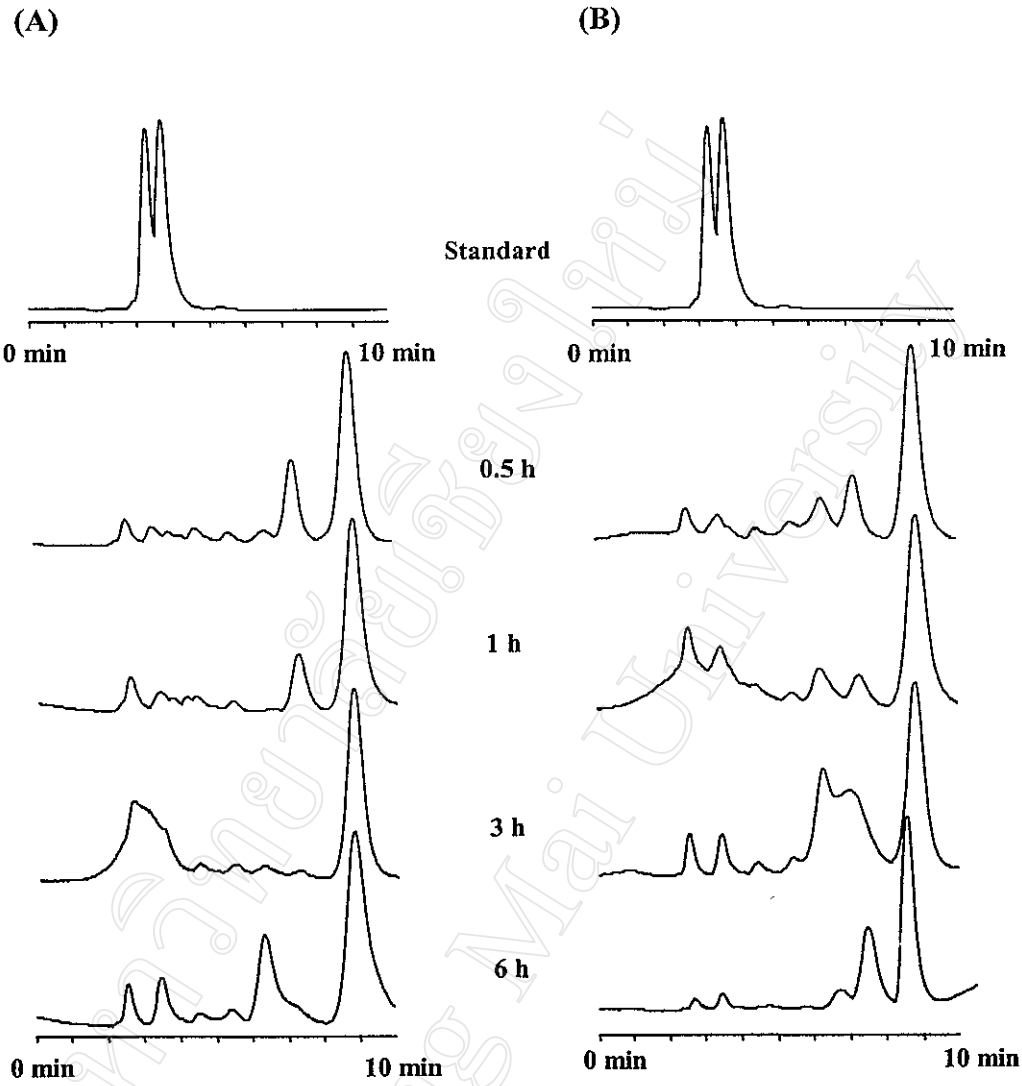

Fig. 3.29. Analysis of unreacted starting material of 3-phenoxy-1,2-propanediol catalyzed with lipase from *B. stearothermophilus* P1 in dichloromethane at room temperature (A) and 55°C (B) for 0.5, 1, 3 and 6 h by Chiralcel OD-RH.

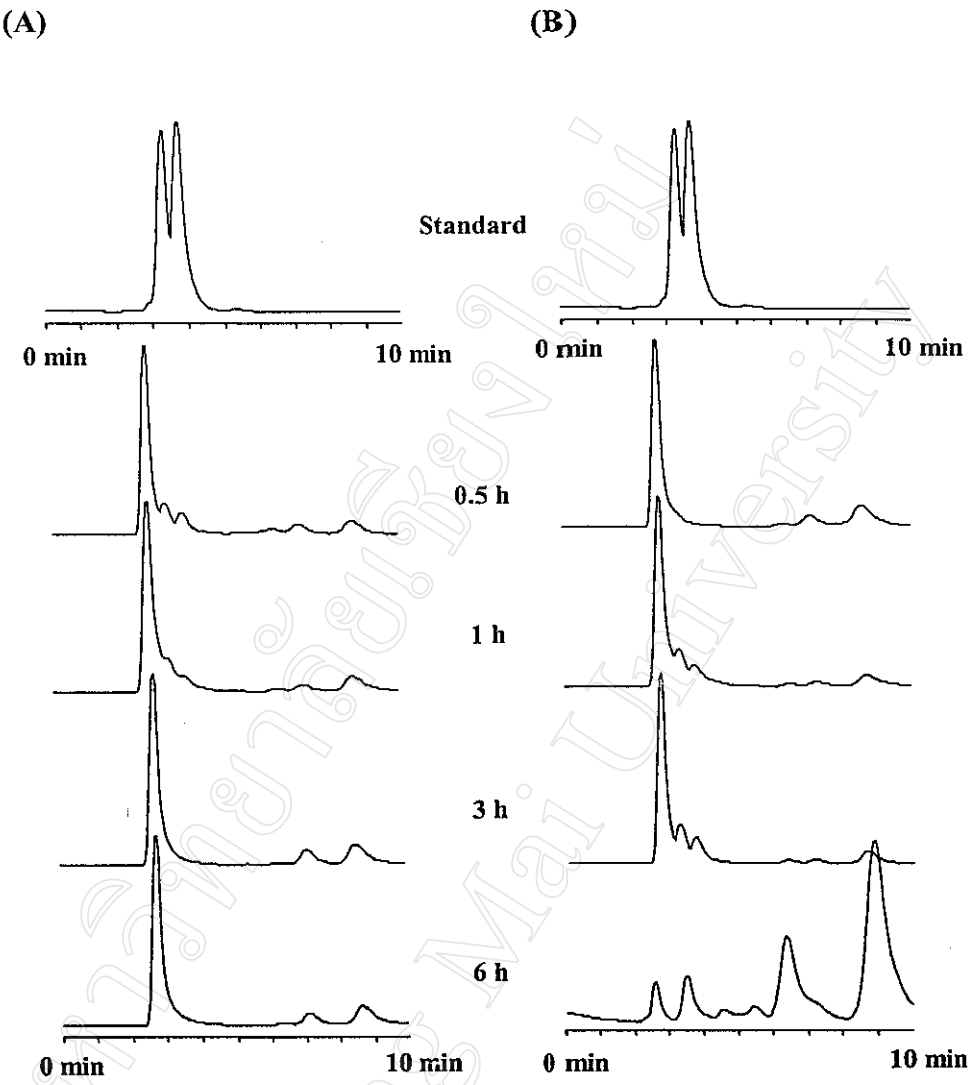

Fig. 3.30. Analysis of unreacted starting material of 3-phenoxy-1,2-propanediol catalyzed with lipase from *B. stearothermophilus* P1 in iso-octane at room temperature (A) and 55°C (B) for 0.5, 1, 3 and 6 h by Chiralcel OD-RH.

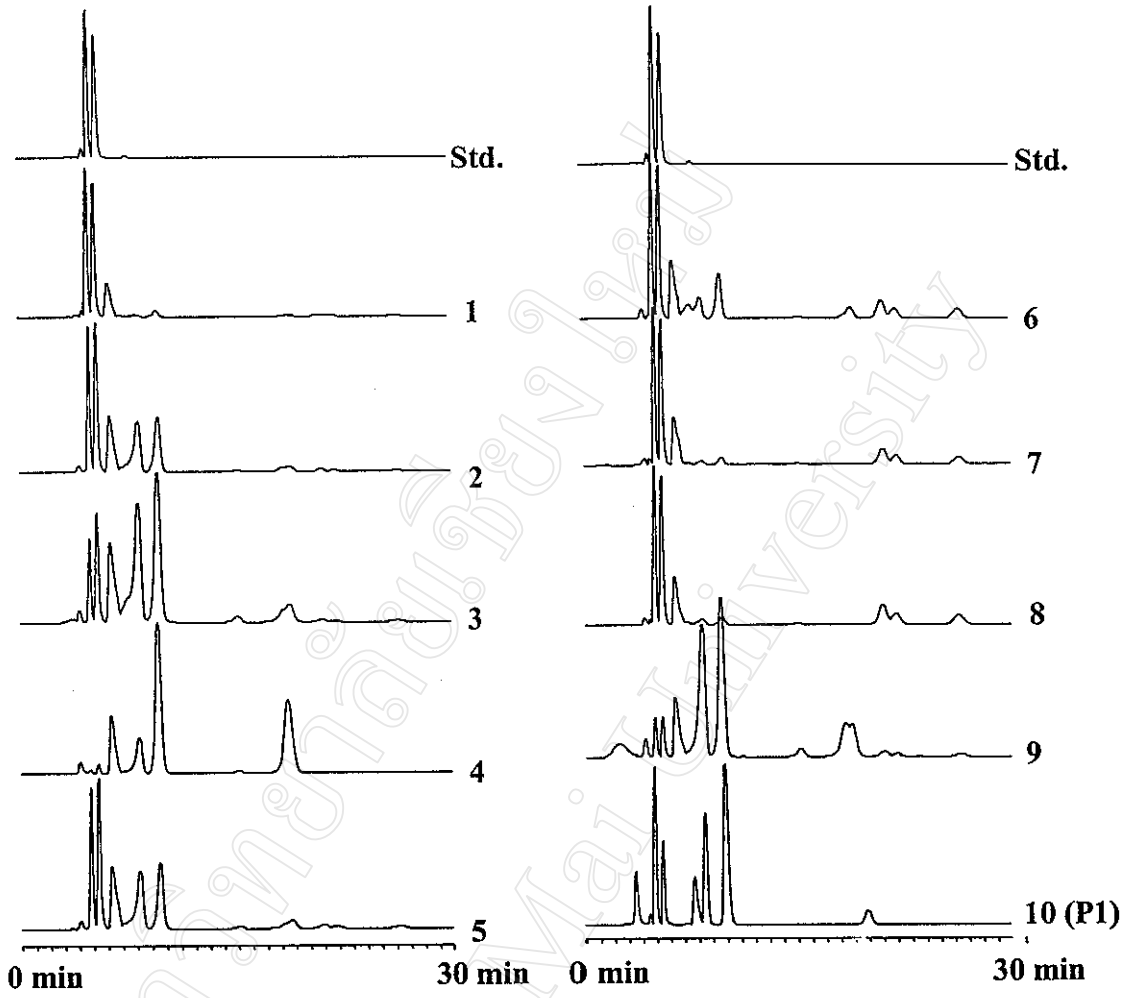

Fig. 3.31. Analysis of unreacted starting material of 3-phenoxy-1,2-propanediol catalyzed with various lipases in dichloromethane at room temperature for 1 h by Chiralcel OD-RH. Labels: Std., standard of 3-phenoxy-1,2-propanediol; 1, lipase AP6 (*Aspergillus niger*, Amano); 2, lipase AY-30 (*Candida cylindracea*, Amano); 3, lipase from *Candida cylindracea* (Meito-Sangyo); 4, lipase GC4 (*Geotrichum candidum*, Amano); 5, lipase MAP (*Mucor meihei*, Amano); 6, lipase N (*Rhizopus niveus*, Amano); 7, lipase R (*Humicola* sp., Amano); 8, lipase R-10 (*Humicola lanuginose*, Amano); 9, lipase L1754 (*Candida rugosa*, Sigma); 10, lipase from *B. stearothermophilus* P1.